Available online at www.sciencedirect.com

ScienceDirect

Ceramics International 40 (2014) 16041–16050

CERAMICS INTERNATIONAL

www.elsevier.com/locate/ceramint

Effect of Fe-doping on structural, magnetic and magnetocaloric properties of $Nd_{0.67}Ba_{0.33}Mn_{1-x}Fe_xO_3$ manganites

Sobhi Hcini[a,*], Michel Boudard[b], Sadok Zemni[a], Mohamed Oumezzine[a]

[a]Laboratoire de Physico-chimie des Matériaux, Faculté des Sciences de Monastir, Département de Physique, Université de Monastir, Monastir 5019, Tunisie
[b]Laboratoire des Matériaux et du Génie Physique, Grenoble INP, CNRS (UMR 5628), MINATEC, 3 parvis Louis Néel, BP 257, 38016 Grenoble Cedex 1, France

Received 7 July 2014; received in revised form 23 July 2014; accepted 25 July 2014
Available online 2 August 2014

Abstract

We have investigated the effect of Fe doping on structural, magnetic and magnetocaloric properties of $Nd_{0.67}Ba_{0.33}Mn_{1-x}Fe_xO_3$ ($0 \le x \le 0.1$) manganites prepared by solid state reaction method at 1673 K. XRD analysis shows that doping Mn by Fe do not affect the crystal structure of samples due to the same ionic radii of Fe^{3+} and Mn^{3+} and hence do not influence physical properties of samples. Magnetization measurements show a ferromagnetic behavior for $x=0$ and 0.02 samples, whereas compounds with $x \ge 0.05$ present a magnetic glass state (cluster or spin glass). The magnetic entropy change was also studied through the examination of measured magnetic isotherms $M(H, T)$ near T_C. The maximum magnetic entropy change ($|\Delta S_M^{max}|$) and the relative cooling power (RCP) are respectively 3.91 and 2.97 J Kg^{-1} K^{-1} and 265 and 242 J Kg^{-1} at a field change of 5 T, for $x=0$ and 0.02 samples. These values are compared favorably with those of some others reported manganites, making our samples promising candidates for the magnetic refrigeration. The field dependence of the magnetic entropy change analysis shows a power law dependence, $\Delta S_M(H) = a(\mu_0 H)^n$, with $n=0.59$ and 0.64 respectively for $x=0$ and 0.02 samples at their respective transition temperatures.

Keywords: Manganites; XRD analysis; Magnetic and magnetocaloric properties

1. Introduction

Recently, perovskite ABO_3-type manganites with the general formula $(R^{3+}_{1-x}A^{2+}_x)(Mn^{3+}_{1-x}Mn^{4+}_x)O^{2-}_3$ (R=La, Pr, Nd..., A=Ca, Sr, Ba...) have been the subject matter of a large number of recent studies due to their interesting physical properties such as colossal magnetoresistance (CMR) and magnetocaloric effect (MCE) [1]. These CMR and MCE properties are usually explained by the double exchange (DE) interaction between the trivalent (Mn^{3+}) and tetravalent (Mn^{4+}) ions [2]. Among mixed-valence manganites studied so far, the $Nd_{0.67}A_{0.33}MnO_3$ system having relatively low single electron band width, exhibits interesting phenomena different from those observed in $La_{1-x}A_xMnO_3$ systems, probably due to the weakening of the DE interaction caused by the larger lattice distortion due to the replacement of Nd with La [3,4].

Perovskite manganites materials have been widely investigated not only for the variety of their physical properties, but also for their potential applications for instance magnetic refrigeration (MR) technology which is based on the MCE. Comparing with the gas compression refrigeration, this technology exhibits significant advantages such as high efficiency and minimal environmental impact [5,6]. The MCE that results from the application or removal of a magnetic field to a magnetic material is characterized by the isothermal entropy change ΔS_M and the adiabatic temperature change ΔT_{ad}.

Recently, a large magnetic entropy change was reported for many compounds such as Gd and Gd–Si–Ge [7,8], $MnFeP_{1-x}As_x$ [9], $LaFe_{13-x}Si_x$ [10], and Ni–Mn–Ga [11]. Hence, research in the magnetic cooling field has been focusing on the search for new materials that are cheaper but displaying larger MCE. In this case, the perovskite manganites are explored to be potential candidates for magnetic refrigeration applications due to their large MCE that is comparable to the entropy change in Gd (see [12] for a review and references

*Corresponding author.
E-mail address: hcini_sobhi@yahoo.fr (S. Hcini).

http://dx.doi.org/10.1016/j.ceramint.2014.07.140

therein), lower cost, simple preparation methods and higher chemical stability. However, the MCE properties of these compounds are variable according to the doping element of the A- and/or B-site. In particular, these properties can be affected by partial replacement of Mn ions by some transition metals such as Al, Fe, Co and Ni [13–17]. It is observed in Ref. [13–17] that the magnetization, the Curie temperature T_C and the magnetic entropy change ΔS_M decrease with increasing the amount of Al, Fe, Co and Ni at Mn site.

Due to the lack of many investigations on properties of Nd-based manganites, we choose to study in this work manganites derived from $Nd_{0.67}Ba_{0.33}MnO_3$. We prepared manganite samples with nominal composition $Nd_{0.67}Ba_{0.33}Mn_{1-x}Fe_xO_3$ ($0 \le x \le 0.1$) using the solid state reaction method and studied the effect of Fe substitution on their structural, magnetic and magnetocaloric properties.

2. Experimental

Samples with nominal compositions $Nd_{0.67}Ba_{0.33}Mn_{1-x}Fe_xO_3$ ($0 \le x \le 0.1$) were prepared by solid state reaction method using stoichiometric amounts of Nd_2O_3, $BaCO_3$, MnO_2 and Fe_2O_3 as precursors, all with purity better than 99.9%. The samples are finally annealed at 1673 K for 48 h in air. Their microstructure and composition were analyzed by scanning electron microscopy (SEM) using a Philips XL30 microscope with an energy dispersive X-ray (EDX) spectrometer working at 20 kV. Powder X-ray diffraction (XRD) were collected using Cu-Kα_1 radiation in the 2θ range 15–130° with a step size of 0.008° and a counting time of 142.3 s per step at room temperature (RT). Rietveld structure refinement was carried out using the FULLPROF software [18]. Magnetization measurements were performed using an extraction magnetometer. The temperature dependence of the magnetization in field cooled (FC) and zero field cooled (ZFC) regimes, $M(T)$, was measured in the range 10–300 K under a constant magnetic field ($\mu_0 H = 0.05$ T). The field dependence of the magnetization, $M(H)$, was measured at 10 K with variable field $\mu_0 H$ up to 10 T. Isothermal $M(H, T)$ data were measured for $x=0$ and 0.02 samples in different temperature ranges around T_C by a step of 3 K under an applied magnetic field varying from 0 to 1 T by step of 0.1 T and from 1 to 5 T by step of 0.5 T.

3. Results and discussions

3.1. Microstructure and structural analysis

A typical example (XRD on samples with $x=0$ and 0.1) of the observed and calculated diffraction profiles obtained from the Rietveld analysis is shown in Fig. 1. The SEM micrographs are given in the insets of this figure. One observes in these micrographs a major primary phase with homogeneous gray contrast and chemical composition (estimated by semi-quantitative EDX analyses) close to the nominal one and a minor secondary phase with white contrast (marked by ∇) with composition close to $Nd(OH)_3$. Results of EDX analysis (not indicated in this figure) on 100 μm × 100 μm regions of samples show that Nd, Ba, Mn and Fe compositions are close to the nominal ones.

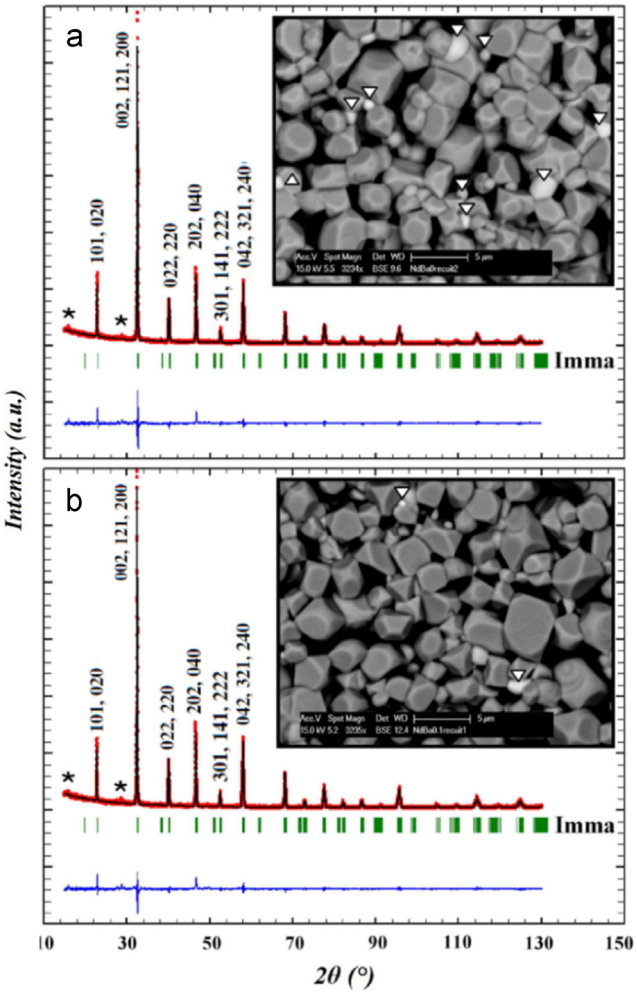

Fig. 1. XRD Rietveld refinement results for samples with (a) $x=0$ and (b) $x=0.1$ at RT showing the presence of a manganite as the majority phase and a minor secondary phase identified as Neodymium Hydroxide $Nd(OH)_3$ phase. All peaks of the manganite phase are indexed in the orthorhombic *Imma* symmetry. Small extra peaks of the secondary phase are marked by asterisk in black color. The difference between measured (red color) and calculated data (black color) is plotted in the bottom (blue color). Green bars correspond to Bragg positions. The insets show SEM image (backscattered electron mode) for $x=0$ and 0.1 compounds. One observes a major primary phase with homogeneous gray contrast and chemical composition (estimated by semi-quantitative EDX analyses) close to the nominal one and a minor secondary phase (marked by ∇) with white contrast and composition close to $Nd(OH)_3$. (For interpretation of the references to color in this figure legend, the reader is referred to the web version of this article.)

Indexing of the XRD patterns and Rietveld structure refinement were performed using the orthorhombic *Imma* symmetry (see Fig. 1). In this refinement, the Whycoff atomic positions are considered as follows: (Nd, Ba) at 4e (0, 1/4, z), (Mn, Fe) at 4b (0, 0, 1/2), O (1) at 4e (0, 1/4, z) and O (2) at 8g (1/4, y, 3/4). Detailed results of Rietveld refinement are listed in Table 1. One can see in this table that all the structural parameters including cell parameters, volume, average bond length $< d_{TM-O} >$ and average bond angle $< \theta_{TM-O-TM} >$ are almost the same for the different samples giving no

Table 1
Structural parameters of XRD Rietveld refinement for $Nd_{0.67}Ba_{0.33}Mn_{1-x}Fe_xO_3$ at RT (*Imma* space group). *V*: cell volume; B_{iso}: isotropic Debye–Waller factor; $< d_{TM-O} >$: average bond lengths between TM=(Mn, Fe) and O; $< \theta_{TM-O-TM} >$: average bond angles; G_s: average grain size. R_p, R_{wp}, and R_F are the agreement factors for the profiles, the weighted profiles and the structure factors; χ^2 is the goodness of fit. The numbers in parentheses are estimated standard deviations to the last significant digit.

	Fe content			**0**	**0.02**	**0.05**	**0.07**	**0.1**
	Space group			Imma				
Cell parameters	a (nm)			0.54915 (1)	0.54917 (1)	0.54923 (1)	0.54927 (1)	0.54929 (1)
	b (nm)			0.77591 (0)	0.77602 (1)	0.77609 (1)	0.77613 (1)	0.77624 (1)
	c (nm)			0.55193 (1)	0.55196 (4)	0.55201 (1)	0.55203 (1)	0.55207 (1)
	V **(*nm*^{3})**			0.23517 (5)	0.23523 (3)	0.23530 (5)	0.23533 (5)	0.23539 (5)
Atoms	***Nd/Ba***	***At. positions***	***x***	0	0	0	0	0
			y	0.25	0.25	0.25	0.25	0.25
			z	−0.0001 (6)	−0.0002 (5)	−0.0004 (6)	−0.0004 (6)	−0.0003 (6)
	Nd/Ba	***B_{iso} (nm^2)***		0.0055 (2)	0.0055 (1)	0.0053 (2)	0.0050 (20)	0.0070 (1)
	Mn/Fe	***At. positions***	***x***	0	0	0	0	0
			y	0	0	0	0	0
			z	0.5	0.5	0.5	0.5	0.5
	Mn/Fe	***B_{iso} (nm^2)***		0.0017 (3)	0.0012 (2)	0.0013 (3)	0.0006 (3)	0.0030 (1)
	O (1)	***At. positions***	***x***	0	0	0	0	0
			y	0.25	0.25	0.25	0.25	0.25
			z	0.564 (2)	0.444 (1)	0.445 (2)	0.444 (2)	0.446 (2)
	O (1)	***B_{iso} (nm^2)***		0.024	0.027	0.027	0.022	0.025
	O (2)	***At. positions***	***x***	0.25	0.25	0.25	0.25	0.25
			y	−0.01 (3)	0.011 (2)	0.011 (3)	0.013 (2)	0.012 (3)
			z	0.75	0.75	0.75	0.75	0.75
	O (2)	***B_{iso} (nm^2)***		0.012	0.013	0.010	0.011	0.016
	$d_{TM-O(1)}$ (nm)			0.1972 (2)	0.1965 (1)	0.1964 (1)	0.1965 (1)	0.1963 (2)
Structural parameters	***$d_{TM-O(2)}$ (nm)***			0.1948 (9)	0.1948 (6)	0.1949 (1)	0.1950 (8)	0.1949 (1)
	$\theta_{TM-O(1)-TM}$ (deg)			159.30 (7)	161.90 (5)	162.24 (6)	161.86 (8)	162.53 (6)
	$\theta_{TM-O(2)-TM}$ (deg)			175.43 (4)	175.21 (3)	174.98 (4)	174.07 (3)	174.52 (5)
	$< d_{TM-O} >$ (nm)			0.1960	0.1957	0.1957	0.1958	0.1956
	$< \theta_{TM-O-TM} >$ (deg)			167.37	168.56	168.61	167.97	168.53
	G_s (nm)			177	261	232	248	220
Agreement factors	***R_p (%)***			7.57	5.37	7.19	7.3	7.3
	R_{wp} (%)			9.69	7.73	9.66	9.51	9.45
	R_F (%)			5.57	5.4	5.57	5.43	5.67
	χ^2 (%)			1.79	4.47	1.84	1.85	1.79

systematic change in the average structure as a function of Fe substitution. Indeed according to Jonker and Ahn et al. [19,20], iron enters into samples as Fe^{3+} and will replace the Mn^{3+} ions. Both ions have almost the same ionic radius of 0.645 Å [21], and thus little or no change in the structural parameters is expected. Therefore, all eventual changes in magnetic and magnetocaloric properties should not be governed by the average crystal structure in these iron doped manganites. The average grain size G_s of our samples is obtained by applying the following Rietveld refinement formula:

$$G_s = \frac{180}{\pi\sqrt{IG}} \quad (1)$$

where λ is the X-ray wavelength and *IG* is the Gaussian size parameter given by Rietveld refinement. The G_s values obtained are reported in Table 1 and range from 177 to 261 nm. These values are significantly lower than those shown by SEM micrographs. This difference is due to the fact that each particle observed by SEM consists of several crystallites domains, probably due to the internal stress or defects (vacancies, dislocations) in the particle [22].

3.2. Magnetic properties

ZFC and FC $M(T)$ curves are presented in Fig. 2 and $M(H)$ curves at 10 K are presented in Fig. 3. These two figures show that samples can be divided on two families with different magnetic behaviors:

i. $x=0$ and 0.02 samples exhibit a clear paramagnetic (PM) – ferromagnetic (FM) phase transition at the Curie temperature (T_C), see Fig. 2a. A reasonable estimation of T_C can be obtained, from the ZFC $M(T)$ curves, by determining the minimum value of dM/dT versus T curves, as shown in the inset of Fig. 2a. Our T_C value for undoped compound, 150 K, is close to that reported, $T_C=164$ K, for $Nd_{0.67}Ba_{0.33}MnO_3$ sample [4] and gradually decreases to lower temperatures when the content of Fe increases. These curves show also a spin canted state at low temperature (below 100 K) (Fig. 2a). In our samples, 1 % Fe doping causes a decrease in T_C by approximately 10 K, similar to that observed by Blanco et al. in Refs. [23,24] for $Nd_{0.7}Pb_{0.3}Mn_{1-x}Fe_xO_3$ compounds and quite different from

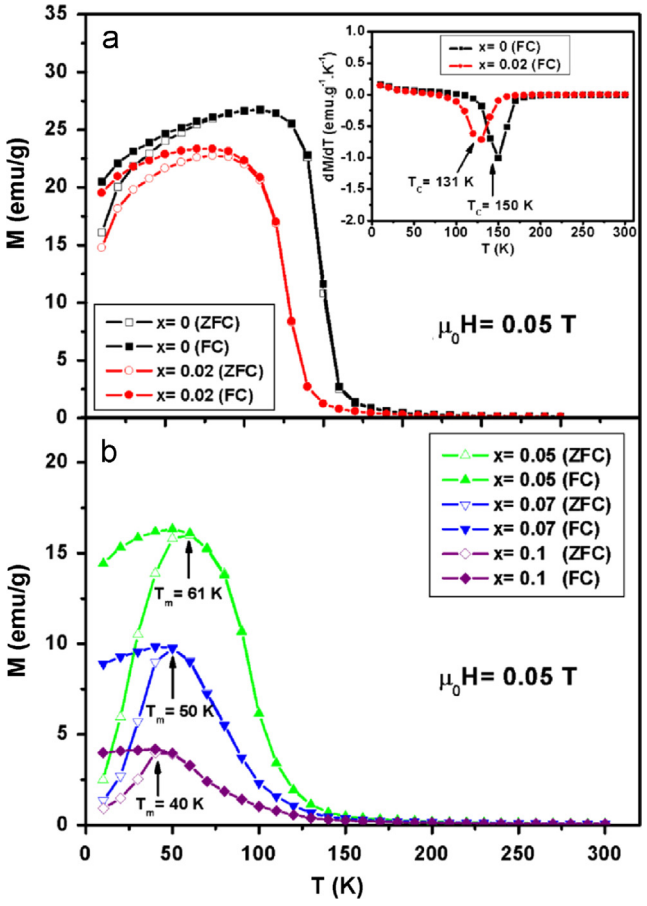

Fig. 2. $M(T)$ curves at $\mu_0 H = 0.05$ T magnetic field in ZFC (open symbols) and FC (close symbols) for $Nd_{0.67}Ba_{0.33}Mn_{1-x}Fe_xO_3$ samples. (a) $M(T)$ curves for $x=0$ and 0.02 samples showing a clear paramagnetic (PM)–ferromagnetic (FM) phase transition at the Curie temperature (T_C) estimated in the inset by determining the minimum value of dM/dT versus T curves. (b) $M(T)$ curves for $x \geq 0.05$ samples showing a magnetic glass state (cluster or spin glass) and a disappearance of the PM–FM transition, the T_m (indicated by arrow) shows the irreversibility and drop of the magnetization in ZFC mode.

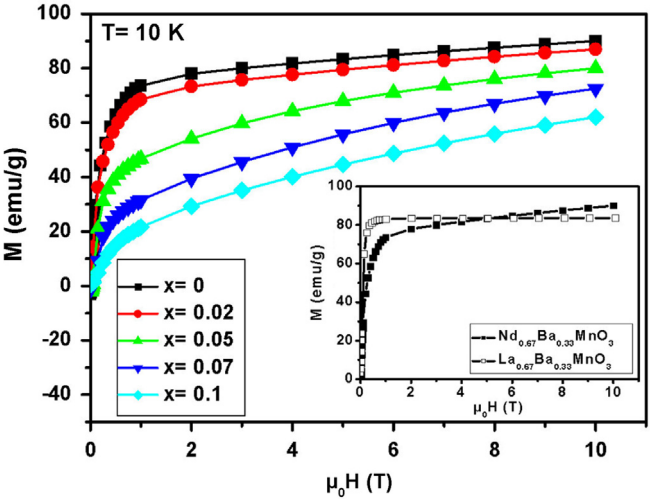

Fig. 3. Magnetization measured at 10 K as a function of the applied field for $Nd_{0.67}Ba_{0.33}Mn_{1-x}Fe_xO_3$ samples showing ferromagnetic behavior for $x=0$ and 0.02 compounds and a superposition of ferromagnetic and antiferromagnetic behaviors for $x \geq 0.05$ compounds. In the inset we compare M (H) curves at 10 K for $La_{0.67}Ba_{0.33}MnO_3$ with non-magnetic rare earth ion (open symbol) [28] and $Nd_{0.67}Ba_{0.33}MnO_3$ with magnetic rare earth (full symbol) [this work].

the obtained for the $Nd_{0.67}Sr_{0.33}Mn_{1-x}Fe_xO_3$ system [25,26], where a drop of 18 K per 1% Fe was observed. The corresponding $M(H)$ curves at 10 K (Fig. 3) show a FM regime with a sharp increase of M at low field (<1 T) corresponding to rearrangement of ferromagnetic domains.

ii. For $x \geq 0.05$ samples, the $M(T)$ curves have no sharp increase and a low magnitude of magnetization is observed (Fig. 2b). At a temperature T_m, indicated by arrow in Fig. 2b, a bifurcation between the FC and ZFC curves (λ shape) is observed which is generally associated in the literature of manganites with a glass magnetic state, with a spin- or cluster-like freezing process that can be related to a loss of ferromagnetic double exchange interaction [27,28]. The corresponding $M(H)$ curves at 10 K (Fig. 3) show that M do not exhibits a FM regime as there is neither a sharp increase and nor a saturation value of M with the applied field that could correspond to parallel spin alignment. This can be attributed to that the increase of Fe content ($x \geq 0.05$) gives rise to an antiferromagnetic coupling between Mn and Fe ions and consequently the DE is progressively suppressed, weakening the FM behavior of our samples [25,26,29]. Similar results were observed by Blanco et al. which showed a spin glass behavior arising from competing FM and AFM interactions in their $Nd_{0.7}Pb_{0.3}Mn_{1-x}Fe_xO_3$ system [23,24]. In particular, the authors in Refs. [23,24], show that the sample with x=0.075 Fe content exhibits a behavior reminiscent of FM to AFM phase transition (typically observed in $Pr_{0.5}Sr_{0.5}MnO_3$ [30]) and their $x=0.1$ sample presents very similar λ shape as our non FM samples. A complex magnetic state due to a mixture of AFM and FM sate is also observed for $Nd_{0.67}A_{0.33}MnO_3$ (A=Ca, Sr, Pb and Ba) samples [3].

The inset of Fig. 3 shows that the magnetization of a similar sample, where magnetic cation Nd^{3+} [Xe $4f^3$] is replaced by non magnetic La^{3+} [Xe], rapidly reaches saturation for $\sim$1 T magnetic field ([28]). The additional magnetic contribution in our sample may be due either to canted long range ordering of the Mn/Nd spins and/or to a magnetic disorder state of Nd (in this scenario the external field induces an additional polarization of Nd superimposed to the one due to the internal field due to Mn spins). This additional contribution can be evaluated at 10 K and 10 T to be of the order of 0.27 μ_B for $x=0$ sample by comparing μ_s^{meas} (3.94 μ_B/f.u. see Table 2) with the calculated value from a full spin alignment of the Mn^{3+} and Mn^{4+} ions (3.67 μ_B/f.u. see Table 2)[1].

To compare experimental and calculated saturation magnetization we have approximated the value of M measured in

[1]Recently it has been reported that μ_s^{meas} of $La_{0.67}Ba_{0.33}MnO_3$ undergoes a very close value (3.61 μ_B /f.u.) to the calculated one (3.67 μ_B /f.u.) as expected from Mn unique contribution [28].

Table 2
Magnetic transition temperature (T_C or T_m); experimental and calculated magnetic saturation moments μ_s^{meas} and μ_s^{cal}; Curie–Weiss temperature Θ; experimental (μ_{eff}^{meas}) and calculated (μ_{eff}^{th}) effective paramagnetic moments for $Nd_{0.67}Ba_{0.33}Mn_{1-x}Fe_xO_3$ samples.

X	T_C or T_m (K)	$\mu_s^{cal}(\mu_B/f.u.)$	$\mu_s^{meas}(\mu_B/f.u.)$	Θ (K)	$\mu_{eff}^{meas}(\mu_B)$	$\mu_{eff}^{th}(\mu_B)$
0	150	3.67	3.94	166	7.02	5.46
0.02	131	3.49	3.81	147	6.92	5.48
0.05	61	3.22	3.50	126	6.79	5.51
0.07	50	3.04	3.17	115	6.78	5.53
0.1	40	2.77	2.72	103	6.56	5.56

10 T at 10 K as the measured saturation magnetization M_s^{meas}. The measured saturation moment expressed in Bohr magneton per atomic formula unit given in Table 2 can be calculated using the following formula:

$$\mu_s^{meas}(\mu_B/f.u.) = M_s^{meas}\, M_m/N_a\, \mu_B \quad (2)$$

with N_a the Avogadro number, M_m the molecular mass per unit formula and μ_B the Bohr magneton. μ_s^{meas} can be compared with the theoretical moment μ_s^{cal} calculated for a full spin alignment of Mn ions which are coupled antiferromagnetically with Fe^{3+} ions, as reported by Mössbauer spectroscopy studies [31,32], neglecting the small contribution of Nd^{3+} spin and orbital moments, in the limit T=0 K. The μ_s^{cal} values given in Table 2 have been obtained with the contribution of only magnetic spin moment[2] according to the following formula:

$$\mu_s^{cal}(\mu_B/f.u.) = (0.67-x)\, M_{Mn^{3+}} - x\, M_{Fe^{3+}} + 0.33\, M_{Mn^{4+}} = 2\,\mu_B\left[(0.67-x)\times\tfrac{4}{2} - x\times\tfrac{5}{2} + 0.33\times\tfrac{3}{2}\right] \quad (3)$$

One can see from Table 2 that the observed and calculated moments coincide reasonably, which confirms that, despite Fe substitution for Mn the FM behavior is weakened.

The inverse of the susceptibility, calculated from $M(T)$ data, as a function of temperature in the PM region (above T_C or T_m) is shown in Fig. 4. It can be generally fitted by the Curie Weiss law:

$$\chi = \frac{C}{T-\Theta} \quad (4)$$

with Θ the Curie Weiss temperature and C the Curie constant defined as:

$$C = \frac{1}{3k_B}\frac{N_a}{M_m}\,\mu_{eff}^{meas2}\mu_B^2 \quad (5)$$

where k_B and μ_{eff}^{meas} are respectively the Boltzmann constant and the effective paramagnetic moment. The obtained Θ values (see Table 2) are positive and decrease with Fe content following the same trend of T_C. The positive value of Θ and the low shift with T_C confirms a mean FM interaction between spins for x=0 and 0.02 samples, whereas for $x \geq 0.05$ samples the shift between Θ and T_m becomes bigger in agreement with the weak ferromagnetism for these samples. The calculated effective moment can be compared with the measured one using the following formula:

where,

$$\mu_{eff}^{th}(\mu_B) = \sqrt{0.67[\mu_{eff}^{th}(Nd^{3+})]^2 + (0.67-x)[\mu_{eff}^{th}(Mn^{3+})]^2 + x[\mu_{eff}^{th}(Fe^{3+})]^2 + 0.33[\mu_{eff}^{th}(Mn^{4+})]^2} \quad (6)$$

$\mu_{eff}^{th}(Mn^{3+}) \sim 4.90\mu_B$; $\mu_{eff}^{th}(Mn^{4+}) \sim 3.87\ \mu_B$; $\mu_{eff}^{th}(Fe^{3+}) \sim 5.92\ \mu_B$ and $\mu_{eff}^{th}(Nd^{3+}) \sim 3.62\ \mu_B$.

One finds that the measured effective magnetic moments in the PM regime are significantly larger than the calculated ones (see Table 2). This result is generally attributed to the existence of short range FM correlation in the PM state [34,35].

3.3. Magnetocaloric properties

In addition to $M(T)$ and $M(H)$ studies, magnetic field dependences of magnetization at different temperatures near T_C, $M(H, T)$, in the range of μ_0H=0–5 T have been recorded. Fig. 5 shows the representative data of x=0 and 0.02 samples. The isothermal magnetization M (H, T) magnetic field dependency, measured at different temperatures below T_C, show a non linear behavior with a sharp increase for low field values and a tendency to saturation as field increases reflecting a ferromagnetic behavior. However for $T > T_C$, a drastically decrease of $M(H, T)$ is observed with an almost linear behavior reflecting a paramagnetic behavior, due to the thermal agitation which disrupts the arrangement of the magnetic moments [36].

To determine the nature of the magnetic phase transition (first or second order) for $Nd_{0.67}Ba_{0.33}Mn_{1-x}Fe_xO_3$ (x=0 and 0.02) samples, we presented in Fig. 6 the Arrott plot [37] (μ_0H/M versus M^2). The (μ_0H/M versus M^2) curves exhibit, in the vicinity of T_C, a positive slope indicating that, according to Banerjee criteria [38], the PM–FM phase transition is of second-order.

Based on the thermodynamic theory, the magnetic entropy change (ΔS_M) in the second order magnetic phase transition, arising when the applied magnetic field changes from 0 to H,

[2]The orbital moment is quenched [33], S=2 for Mn^{3+}, S=3/2 for Mn^{4+}, S=5/2 for Fe^{3+} and g=2 for Mn^{3+}, Mn^{4+} and Fe^{3+}.

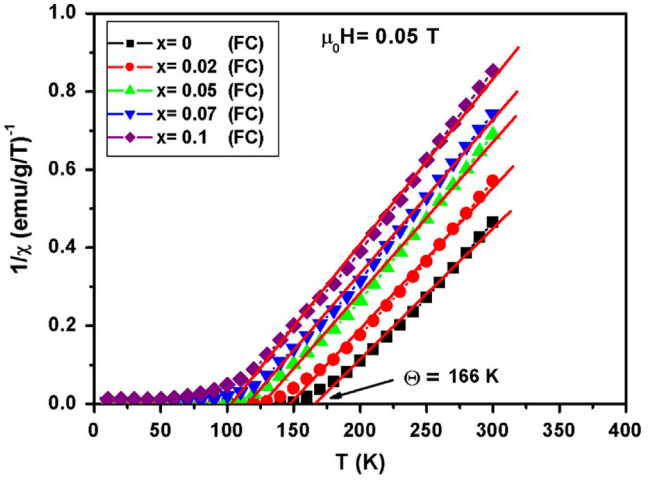

Fig. 4. Temperature dependence of the inverse of the magnetic susceptibility $1/\chi = \mu_0 H/M$ (measured for $\mu_0 H = 0.05$ T) for $Nd_{0.67}Ba_{0.33}Mn_{1-x}Fe_xO_3$ samples.

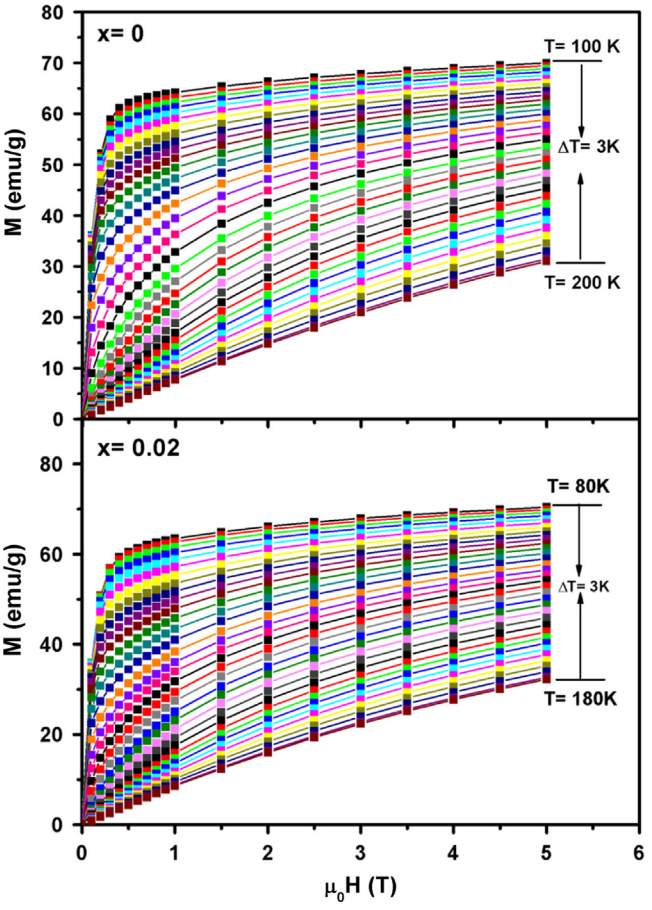

Fig. 5. M (H, T) curves near T_C for $Nd_{0.67}Ba_{0.33}Mn_{1-x}Fe_xO_3$ ($x=0$ and 0.02) samples.

can be derived from the thermodynamic Maxwell relation:

$$\left(\frac{\partial S}{\partial H}\right)_T = \left(\frac{\partial M}{\partial T}\right)_H \tag{7}$$

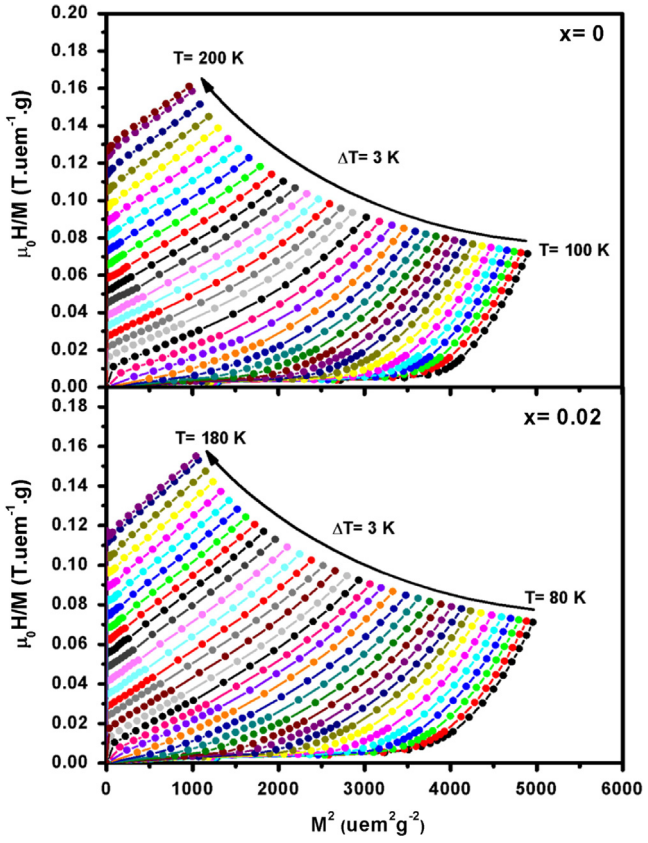

Fig. 6. Arrott plots around T_C for $Nd_{0.67}Ba_{0.33}Mn_{1-x}Fe_xO_3$ ($x=0$ and 0.02) samples.

From the $M(H, T)$ data, the magnetic entropy change for our samples can be calculated as [39]:

$$\Delta S_M(T, \Delta H) = S_M(T,\ H) - S_M(T, 0) = \int_0^H \left(\frac{\partial M}{\partial T}\right)_H dH \tag{8}$$

In the case of magnetization measurements at small discrete field and temperature intervals, numerical approximation to the integral in Eq. (8) could be expressed as [40]:

$$\Delta S_M(T, \Delta H) = \sum \frac{M_i - M_{i+1}}{T_i - T_{i+1}} \Delta H_i \tag{9}$$

where M_i and M_{i+1} are the magnetization values measured under a magnetic field ΔH_i at T_i and T_{i+1} respectively.

Fig. 7 shows the temperature dependences of $\Delta S_M(T, \Delta H)$ for $Nd_{0.67}Ba_{0.33}Mn_{1-x}Fe_xO_3$ ($x=0$ and 0.02) samples at various magnetic fields. As seen from Fig. 7, the ΔS_M exhibits a maximum, $|\Delta S_M^{max}|$, near T_C. This maximum increases with the increase of magnetic field and shifts towards lower temperatures when the Fe content increases, following the same trend of T_C.

The magnetic cooling efficiency of a magnetocaloric material is evaluated by considering the relative cooling power (RCP) [12] given by:

$$RCP = |\Delta S_M^{max}| \times \delta T_{FWHM} \tag{10}$$

where δT_{FWHM} is the fullwidth at half maximum of the magnetic entropy change curve. The $|\Delta S_M^{max}|$ and RCP values

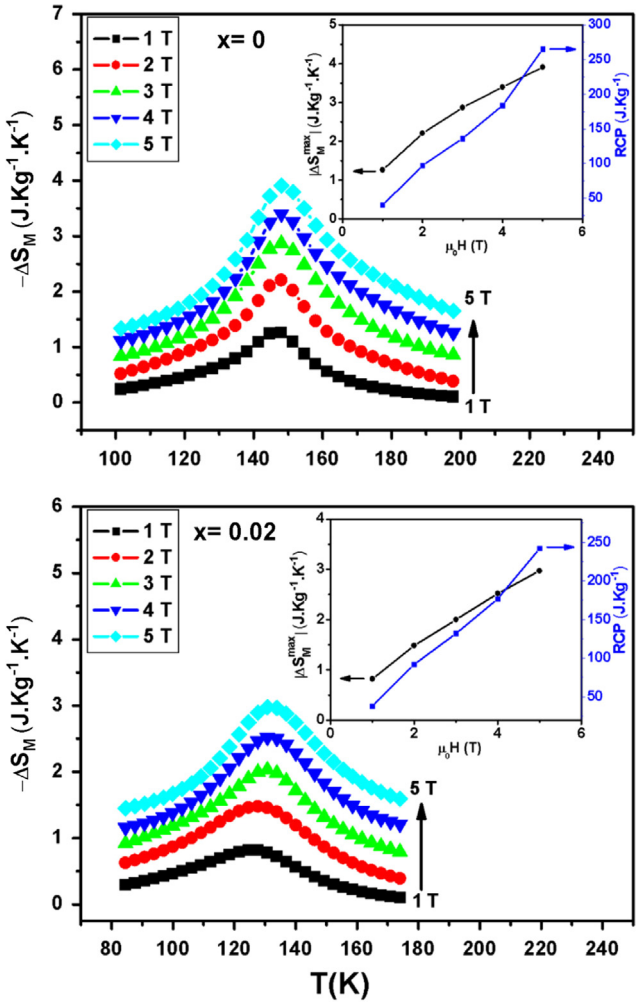

Fig. 7. Temperature dependence of the magnetic entropy change under different amplitudes of change in the magnetic field (from bottom to top ΔH=1 T, 2 T, 3 T, 4 T, and 5 T) for $Nd_{0.67}Ba_{0.33}Mn_{1-x}Fe_xO_3$ (x=0 and 0.02) samples. Insets: dependency of the maximum entropy change $|\Delta S_M^{max}|$ and the relative cooling power RCP with ΔH for x=0 and 0.02 Fe content.

obtained for x=0 and 0.02 Fe content exhibit an almost linear rise with increasing ΔH as exemplified in the insets of Fig. 7. We compared in Table 3 the performances of magnetocaloric effect corresponding to a magnetic field of 5 T of our samples with some others reported in the literature. As can be seen from Table 3 our RCP values for x=0 and 0.02 samples are respectively about 65% and 59% of that of pure Gd [7,8] under ΔH=5 T. However we note that our $Nd_{0.67}Ba_{0.33}Mn_{1-x}Fe_xO_3$ (x=0 and 0.02) samples can thus be used as an active magnetic refrigerator. Table 3 shows also, that the values achieved in our work are in good agreement with those reported in Ref. [13,14]. Especially, the authors showed that the incorporation of Fe at Mn-site reduced the maximum entropy change $|\Delta S_M^{max}|$ in samples [13,14]. A similar behavior was observed for homologous transition metals-doped $La_{1-x}Sr_xMn_{1-x}M_xO_3$ manganites (M=Al, Ni and Co) [15–17].

In our samples, the reduction of magnetocaloric properties, i.e. the decrease of T_C, $|\Delta S_M^{max}|$ and RCP values, when increasing Fe content can be explained qualitatively by the reduction of the Mn^{3+}/Mn^{4+} ratio which decreases from 2.030 (for x=0) to 1.970 (for x=0.02). This effect reduces the Mn^{3+}–Mn^{4+} couples which are responsible of DE ferromagnetism and introduces a little proportion of Mn^{3+}–Mn^{3+}, Mn^{4+}–Mn^{4+}, Fe^{3+}–Fe^{3+} and Mn^{3+}–Fe^{3+} couples which enhances SE antiferromagnetic state.

The change of magnetic entropy can be also calculated from the field dependence of the specific heat by the following integration [12]:

$$\Delta S_M(T,H) = \int_0^T \frac{C_p(T,\mu_0 H) - C_p(T,0)}{T} dT \tag{11}$$

The change of specific heat ΔC_p associated with a magnetic field variation from 0 to H can be calculated using Eq. (11) as:

$$\Delta C_p(T,\mu_0 H) = C_p(T,\mu_0 H) - C_p(T,0) = T\frac{\partial(\Delta S_M(T,\mu_0 H))}{\partial T} \tag{12}$$

Using Eq. (12), ΔC_p of the $Nd_{0.67}Ba_{0.33}Mn_{1-x}Fe_xO_3$ (x=0 and 0.02) samples versus temperature at different magnetic fields is displayed in Fig. 8. As the figure shows, anomalies are observed in all curves around the Curie temperature T_C, which are due to the magnetic phase transition. The value of ΔC_p undergoes a sudden change of sign from positive to negative around T_C with a negative value below T_C and a positive value above T_C. In addition, the maximum/minimum values of ΔC_p exhibit a monotonic increase with increasing ΔH and are observed at temperatures 155/141 and 143/122 respectively for x=0 and 0.02 samples.

According to Oesterreicher and Parker [43], the field dependence of the magnetic entropy change (ΔS_M) at a temperature T of materials with a second order PM–FM phase transition follows an exponent power law:

$$\Delta S_M(H) = a(\mu_0 H)^n \tag{13}$$

where a is a constant and the exponent "n" depends on the magnetic state of the sample. In the mean field approach, the value of n at T_C is predicted to be 2/3 [43]. On the other hand, recent experimental results show a deviation from n=2/3 in the case of some manganites materials [44]. By fitting the data of ΔS_M versus ΔH at each temperature to Eq. (13), we obtain the value of n as a function of temperature, as depicted in Fig. 9. It can be noted from Fig. 9 that the value of n exhibits a sudden change around T_C. It decreases with increasing temperature in the FM region (below T_C) with a minimum value near T_C and increases with increasing temperature in the PM region (above T_C). The n values around T_C are 0.59 and 0.64 respectively for x=0 and 0.02 samples. It can be seen that the value of n obtained for x=0.02 sample, is in good agreement with the mean field prediction n=2/3 [43]. As against, for x=0 sample, this value is lower than 2/3. This deviation from the mean field behavior (for x=0 sample) can be attributed to the presence of local inhomogeneities in the vicinity of transition temperature [45]. On the other hand, our

Table 3
Maximum entropy change $|\Delta S_M^{max}|$ and relative cooling power (RCP) occurring at the Curie temperature T_C and at a magnetic field $\Delta H = 5\ T$ for $Nd_{0.67}Ba_{0.33}Mn_{1-x}Fe_xO_3$ ($x=0$ and 0.02) samples compared to several materials considered for magnetic refrigeration.

Composition	T_C (K)	ΔH (T)	$\lvert \Delta S_M^{max} \rvert$ ($J\ Kg^{-1}\ K^{-1}$)	RCP ($J\ Kg^{-1}$)	Ref.
Gd	293	5	9.5	410	[7]
$La_{0.67}Ba_{0.33}MnO_3$	292	5	1.48	161	[41]
$La_{0.67}Ba_{0.33}MnO_3$	332	5	3.51	235	[13]
$Pr_{0.67}Ba_{0.33}MnO_3$	205	5	4.37	230	[13]
$Nd_{0.67}\ Ba_{0.33}MnO_3$	145	5	3.91	265	This work
$La_{0.67}\ Ba_{0.33}Mn_{0.98}Ti_{0.02}O_3$	314	5	3.24	307	[42]
$Nd_{0.67}\ Ba_{0.33}Mn_{0.98}Fe_{0.02}O_3$	134	5	2.97	242	This work
$La_{0.67}Ba_{0.33}Mn_{0.95}Fe_{0.05}O_3$	271	5	2.54	246	[13]
$Pr_{0.67}Ba_{0.33}Mn_{0.95}Fe_{0.05}O_3$	128	5	3.09	287	[13]
$La_{0.7}Sr_{0.3}Mn_{0.95}Fe_{0.05}O_3$	343	5	4.4	215	[14]
$La_{0.7}Sr_{0.3}Mn_{0.95}Al_{0.05}O_3$	332	5	4.4	–	[15]
$La_{0.67}Sr_{0.33}Mn_{0.95}Ni_{0.05}O_3$	–	5	3.2	–	[16]
$La_{0.7}Sr_{0.3}Mn_{0.93}Fe_{0.07}O_3$	296	5	4.0	225	[14]
$La_{0.67}Sr_{0.33}Mn_{0.9}Ni_{0.1}O_3$	290	5	3	132	[16]
$La_{0.67}Sr_{0.33}Mn_{0.9}Co_{0.1}O_3$	328	5	5.00	200	[17]

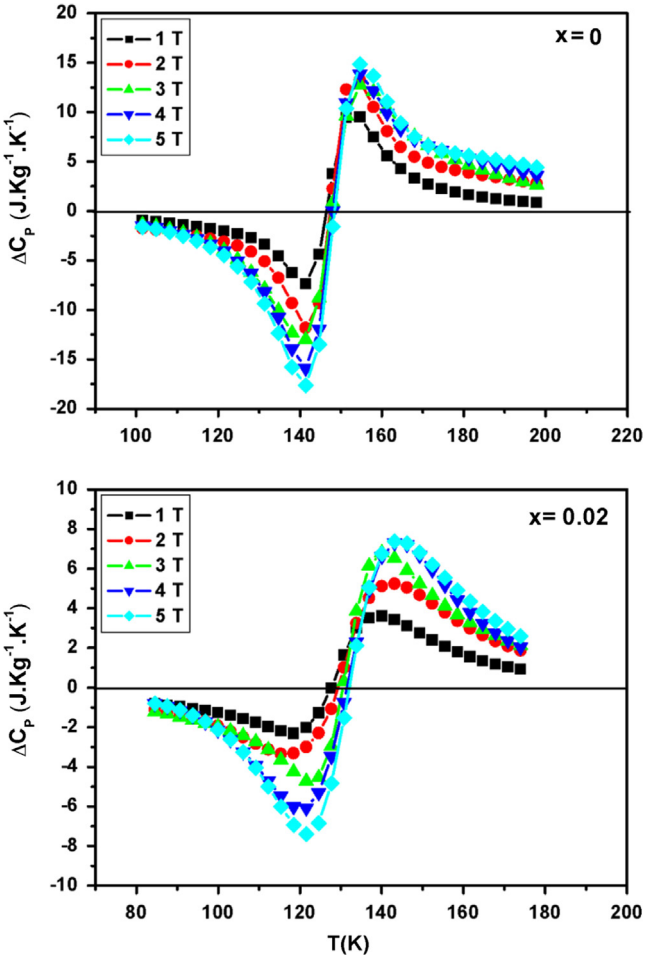

Fig. 8. Change of specific heat ΔC_p of $Nd_{0.67}Ba_{0.33}Mn_{1-x}Fe_xO_3$ ($x=0$ and 0.02) samples as a function of temperature at different magnetic fields.

values are similar to those obtained for soft magnetic alloys, gadolinium (Gd) and other magnetic materials containing rare earth metals [46–49].

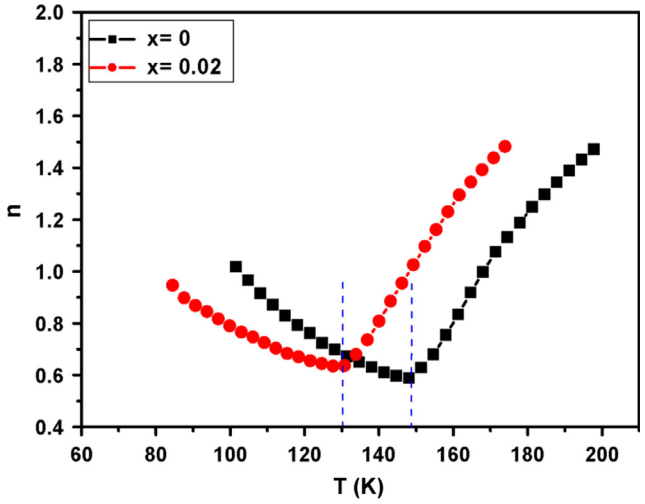

Fig. 9. Temperature dependence of the exponent n for $Nd_{0.67}Ba_{0.33}Mn_{1-x}Fe_xO_3$ ($x=0$ and 0.02) samples.

4. Conclusion

We have studied the effect of Fe doping at Mn-site on structural, magnetic and magnetocaloric properties of $Nd_{0.67}Ba_{0.33}Mn_{1-x}Fe_xO_3$ ($0 \le x \le 0.1$) manganites. Powder XRD structure analysis and morphological investigation have shown that structural parameters and grain sizes are slightly affected by Fe doping giving no influence on physical properties which the interpretation should be based on the competition between DE and SE exchange interactions. Magnetic measurements show a ferromagnetic behavior for $x=0$ and 0.02 samples, whereas compounds with $x \ge 0.05$ present a magnetic glass state with a spin- or cluster-like freezing behavior. Magnetocaloric properties show that the maximum magnetic entropy change $|\Delta S_M^{max}|$ and the relative cooling power (RCP) are relatively high for samples with $x=0$ and 0.02 Fe content

making our samples promising materials to be used in ecologically friendly magnetic refrigeration technology. The field dependence of the magnetic entropy variation shows a power law dependence $\Delta S_M(H) = a(\mu_0 H)^n$, with $n=0.59$ and 0.64 respectively for $x=0$ and 0.02 samples.

References

[1] J. Yang, Y.P. Lee, Critical behavior in Ti-doped manganites, Appl. Phys. Lett. 91 (2007) 142512–142514.

[2] C. Zener, Interaction between the *d* shells in the transition metals, Phys. Rev. 81 (1951) 440–444.

[3] D.C. Krishna, Y. Kalyana Lakshmi, B. Sreedhar, P. Venugopal Reddy, Magnetic transport behavior of nanocrystalline $Nd_{0.67}A_{0.33}MnO_3$ (A=Ca, Sr, Pb and Ba), Solid State Sci. 11 (2009) 1312–1318.

[4] G. Venkataiah, P. Venugopal Reddy, Structural, magnetic and magneto-transport behavior of some Nd-based perovskite manganites, Solid State Commun. 136 (2005) 114–119.

[5] O. Tegus, E. Bruck, K.H.J. Buschow, F.R. de Boer, Transition-metal-based magnetic refrigerants for room-temperature applications, Nature 415 (2002) 150–152.

[6] A.M. Tishin, I. Spichkin, The Magnetocaloric Effect and its Applications, Institute of Physics Publishing, Bristol, 2003.

[7] V.K. Pecharsky Jr., K.A. Gschneidner, Effect of alloying on the giant magnetocaloric effect of $Gd_5(Si_2Ge_2)$, J. Magn. Magn. Mater. 167 (1997) L179–L184.

[8] V.K. Pecharsky, K.A. Gschneidner Jr., Giant magnetocaloric effect in $Gd_5(Si_2Ge_2)$, Phys. Rev. Lett. 78 (1997) 4494–4497.

[9] H. Wada, Y. Tanabe, Giant magnetocaloric effect of $MnAs_{1-x}Sb_x$, Appl. Phys. Lett. 79 (2001) 3302–3304.

[10] F.X. Hu, B.G. Shen, J.R. Sun, Z.H. Cheng, G.H. Rao, X.X. Zhang, Influence of negative lattice expansion and metamagnetic transition on magnetic entropy change in the compound $LaFe_{11.4}Si_{1.6}$, Appl. Phys. Lett. 78 (2001) 3675–3677.

[11] F.X. Hu, B.G. Shen, J.R. Sun, Magnetic entropy change in $Ni_{51.5}Mn_{22.7}Ga_{25.8}$ alloy, Appl. Phys. Lett. 76 (2000) 3460–3462.

[12] M.H. Phan, S.C. Yu, Review of the magnetocaloric effect in manganite materials, J. Magn. Magn. Mater. 308 (2007) 325–340.

[13] M. Baazaoui, M. Boudard, S. Zemni, Magnetocaloric properties in $Ln_{0.67}Ba_{0.33}Mn_{1-x}Fe_xO_3$ (Ln=La or Pr) manganites, Mater. Lett. 65 (2011) 2093–2095.

[14] S.K. Barik, C. Krishnamoorthi, R. Mahendiran, Effect of Fe substitution on magnetocaloric effect in $La_{0.7}Sr_{0.3}Mn_{1-x}Fe_xO_3$ ($0.05 \le x \le 0.20$), J. Magn. Magn. Mater. 323 (2011) 1015–1021.

[15] D.N.H. Nam, N.V. Dai, L.V. Hong, N.X. Phuc, S.C. Yu, M. Tachibana, E. Takayama- Muromachi, Room-temperature magnetocaloric effect in $La_{0.7}Sr_{0.3}Mn_{1-x}M'_xO_3$ (M′=Al, Ti), J. Appl. Phys. 103 (2008) 043905–043909.

[16] C.P. Reshmi, S. Savitha Pillai, K.G. Suresh, Manoj Raama Varma, Room temperature magnetocaloric properties of Ni substituted $La_{0.67}Sr_{0.33}MnO_3$, Solid State Sci. 19 (2013) 130–135.

[17] Y. Sun, W. Tong, Y.H. Zhang, Large magnetic entropy change above 300 K in $La_{0.67}Sr_{0.33}Mn_{0.9}Cr_{0.1}O_3$, J. Magn. Magn. Mater. 232 (2001) 205–208.

[18] H.M. Rietveld, A profile refinement method for nuclear and magnetic structures, J. Appl. Crystallogr. 2 (1969) 65–71.

[19] G.H. Jonker, Semiconducting properties of mixed crystals with perovskite structure, Physica 20 (1954) 1118–1122.

[20] K.H. Ahn, X.W. Wu, K. Liu, C.L. Chien, Effects of Fe doping in the colossal magnetoresistive $La_{1-x}Ca_xMnO_3$, J. Appl. Phys. 81 (1999) 5505–5507.

[21] R.D. Shannon, Revised effective ionic radii and systematic studies of interatomic distances in halides and chalcogenides, Acta Crystallogr. A 32 (1976) 751–764.

[22] C. Vázquez-Vázquez, M.C. Blanco, M.A. López-Quintela, R.D. Sánchez, J. Rivas, S.B. Oseroff, Characterization of $La_{0.67}Ca_{0.33}MnO_{3\pm\delta}$ particles prepared by the sol–gel route, J. Mater. Chem. 8 (1998) 991–1000.

[23] J.J. Blanco, M. Insausti, I. Gil de Muro, L. Lezama, T. Rojo, Neutron diffraction and magnetic study of the $Nd_{0.7}Pb_{0.3}Mn_{1-x}Fe_xO_3$ ($0 \leqslant x \leqslant 0.1$) perovskites, J. Solid State Chem. 179 (2006) 623–631.

[24] J.J. Blanco, L. Lezama, M. Insausti, J. Gutierrez, J.M. Barandiaran, T. Rojo, Study of the $Nd_{0.7}A_{0.3}Mn_{1-x}B_xO_3$ (A=Pb, Cd; *B*=Fe, Co, Ni; $x=0$, 0.1) phases: synthesis, characterization, and magnetic properties, Chem. Mater. 11 (1999) 3464–3469.

[25] J. Takeuchi, S. Hirahara, T.P. Dhakal, K. Miyoshi, K. Fujiwara, Colossal magnetoresistance of perovskite $Nd_{0.67}Sr_{0.33}Mn_{1-x}FexO_3$ single crystals, J. Magn. Magn. Mater. 226–230 (2001) 884–885.

[26] Y.L. Chang, Q. Huang, K. Ong, Effect of Fe doping on the magnetotransport properties in manganese oxides, J. Appl. Phys. 91 (2002) 789–793.

[27] J.A. Mydosh, Spin Glass: An experimental Introduction, Taylor & Francis, London, 1993.

[28] M. Baazaoui, S. Zemni, M. Boudard, H. Rahmouni, A. Gasmi, A. Selmi, M. Oumezzine, Magnetic and electrical behaviour of $La_{0.67}Ba_{0.33}Mn_{1-x}Fe_xO_3$ perovskites, Mater. Lett. 63 (2009) 2167–2170.

[29] T.P. Dhakal, K. Miyoshi, K. Fujiwara, J. Takeuchi, Magnetotransport properties of the perovskite $Nd_{0.67}Sr_{0.33}Mn_{1-x}CO_xO_3$ single crystals, J. Magn. Magn. Mater. 226–230 (2001) 824–825.

[30] W. Boujelben, A. Cheikh-Rouhou, J. Pierre, J.C. Joubert, Effect of quenching on magnetic properties of polycrystalline $Pr_{0.5}Sr_{0.5}MnO_3$ perovskite manganite, J. Alloys Compd. 314 (2001) 15–21.

[31] A.G. Mostafa, E.K. Abdel-Khalek, W.M. Daoush, S.F. Moustafa, Study of some co-precipitated manganite perovskite samples-doped iron, J. Magn. Magn. Mater. 320 (2008) 3356–3360.

[32] S.B. Ogale, R. Shreekala, R. Bathe, S.K. Date, S.I. Patil, B. Hannoyer, F. Petit, G. Marest, Transport properties, magnetic ordering, and hyperfine interactions in Fe-doped $La_{0.75}Ca_{0.25}MnO_3$: localization–delocalization transition, Phys. Rev. B 57 (1998) 7841–7845.

[33] C. Kittel, Introduction to Solid State Physics, sixth ed., Wiley, New York, pp. 404–406.

[34] S. Hcini, M. Boudard, S. Zemni, Study of Na substitution in $La_{0.67}Ba_{0.33}MnO_3$ perovskites, Appl. Phys. A 115 (2014) 985–996.

[35] A. Gasmi, M. Boudard, S. Zemni, F. Hippert, M. Oumezzine, Influence of non-magnetic Ti^{4+} ion doping at Mn site on structural and magnetic properties of $La_{0.67}Ba_{0.33}MnO_3$, J. Phys. D: Appl. Phys. 42 (2009) 225408–225414.

[36] Brahim Arayedh, Sami Kallel, Nabil Kallel, Octavio Peña, Influence of non-magnetic and magnetic ions on the MagnetoCaloric properties of $La_{0.7}Sr_{0.3}Mn_{0.9}M_{0.1}O_3$ doped in the Mn sites by M=Cr, Sn, Ti, J. Magn. Magn. Mater. 361 (2014) 68–73.

[37] A. Arrott, Criterion for ferromagnetism from observations of magnetic isotherms, Phys. Rev. 108 (1957) 1394–1396.

[38] S.K. Banerjee, On a generalised approach to first and second order magnetic transitions, Phys. Lett. 12 (1964) 16–17.

[39] X. Bohigas, J. Tejada, M.L. Marinez-Sarrion, S. Tripp, R. Black, Magnetic and calorimetric measurements on the magnetocaloric effect in $La_{0.6}Ca_{0.4}MnO_3$, J. Magn. Magn. Mater. 208 (2000) 85–92.

[40] R.D. McMichael, J.J. Ritter, R.D. Shull, Enhanced magnetocaloric effect in $Gd_3Ga_{5-x}Fe_xO_{12}$, J. Appl. Phys. 73 (1993) 6946–6948.

[41] D.T. Morelli, A.M. Mance, J.V. Mantese, A.L. Micheli, Magnetocaloric properties of doped lanthanum manganite films, J. Appl. Phys. 79 (1996) 373–375.

[42] Ma. Oumezzine, S. Zemni, O. Peña, Room temperature magnetic and magnetocaloric properties of $La_{0.67}Ba_{0.33}Mn_{0.98}Ti_{0.02}O_3$ perovskite, J. Alloys Compd. 508 (2010) 292–296.

[43] H. Oesterreicher, F.T. Parker, Magnetic cooling near Curie temperatures above 300 K, J. Appl. Phys. 55 (1984) 4334–4336.

[44] V. Franco, R. Caballero-Flores, A. Conde, K.E. Knipling, M.A. Willard, Magnetocaloric effect and critical exponents of $Fe_{77}Co_{5.5}Ni_{5.5}Zr_7B_4Cu_1$: a detailed study, J. Appl. Phys. 109 (2011) 07A905-07A907.

[45] Q.Y. Dong, H.W. Zhang, J.R. Sun, B.G. Shen, V. Franco, A phenomenological fitting curve for the magnetocaloric effect of materials with a second-order phase transition, J. Appl. Phys. 103 (2008) 116101–116103.

[46] M. Pękala, Magnetic field dependence of magnetic entropy change in nanocrystalline and polycrystalline manganites $La_{1-x}M_xMnO_3$ (M=Ca, Sr), J. Appl. Phys. 108 (2010) 113913–113916.

[47] C.P. Reshmi, S. Savitha Pillai, M. Vasundhara, G.R. Raji, K.G. Suresh, M. Raama Varma, Co-existence of magnetocaloric effect and magnetoresistance in Co substituted $La_{0.67}Sr_{0.33}MnO_3$ at room temperature, J. Appl. Phys. 114 (2013) 033904–033910.

[48] V. Franco, C.F. Conde, J.S. Blazquez, A. Conde, P. Svec, D. Janickovic, L.F. Kiss, A Constant Magnetocaloric Response in FeMoCuB amorphous alloys with different Fe/B ratios, J. Appl. Phys. 101 (2007) 093903–093907.

[49] P. Nisha, S. Savitha Pillai, M. Raama Varma, K.G. Suresh, Critical behavior and magnetocaloric effect in $La_{0.67}Ca_{0.33}Mn_{1-x}Cr_xO_3$ (x=0.1, 0.25), Solid State Sci. 14 (2012) 40–47.